SWIM: Speed-aware WiFi-based Passive Indoor Localization for Mobile Ship Environment

Mozi Chen, Kezhong Liu, Jie Ma, Yu Gu, *Senior Member, IEEE,* Zheng Dong, *Member, IEEE,* and Cong Liu, *Member, IEEE,*

Abstract—Accurate and pervasive device-free indoor localization with meter-level resolution is critical for large cruise and passenger ships due to safety-critical rescue and evacuation requirements when accidents occur. However, existing localization techniques would severely suffer on ships because of their unique mobility characteristics. In this paper, we take the first attempt to build a ubiquitous passive localization system using WiFi fingerprints for the mobile ship environment. By conducting extensive experiments and measurements during several cruise trips, we identified a major influence factor on the fingerprints in the mobile environment: varying the ship speeds may significantly change the patterns of fingerprints at runtime. Since it may be too expensive to identify the fingerprints associated with different speeds, we propose an efficient localization method, namely SWIM, which calibrates the fingerprints from only a single-speed scenario to multiple-speed scenarios using a signal reconstruction analysis. SWIM is designed to learn the predictive fingerprint variation introduced by environmental speed changes and reconstruct the original fingerprints to adapt to the runtime speed scenarios. We have implemented and extensively evaluated SWIM on actual cruise ships. Experimental results demonstrate that SWIM improves localization accuracy from 63.2% to 82.9%, while reducing the overall system deployment cost by 87%.

Index Terms—Device-free indoor localization, Mobile ship environment, Channel State Information (CSI), WiFi

1 Introduction

Guaranteeing safety at sea has always been of the highest priority in the passenger ship industry ever since the catastrophic RMS Titanic accident in 1912. Recent tragedies (e.g., 442 deaths in the Oriental Star cruise accident in 2015 [1]) have shown that fatal accidents may happen even nowadays, and improving the evacuation and rescue process of a damaged ship is one of the most critical tasks. In the event of such catastrophes, an accurate and pervasive indoor localization supports rescue/evacuation operations and dramatically reduces the time needed to bring the ship under control [2] [3].

Indoor localization is a well-studied research topic [4]. Various systems solutions have been proposed, such as radio-frequency identification (RFID) based systems [5] [6] and WiFi-based systems [7] [8] [9]. In these systems, users need to wear certain devices (e.g., mobile phones or RFID tags) to collect data on their current location. These solutions are considered to be obtrusive to the users. In addition, it is difficult to guarantee that users would wear the equipment when an emergency happens. Therefore, the technique of device-free passive (DfP) detection, which detects objects' locations without attaching any device, has been developed in recent years [10] [11]. With the expansion of wireless networks, it is possible to passively localize people by capturing the radio-frequency (RF) changes caused by human body reflection. Unlike vision-based DfP solutions, RF-based approaches can work at non-line-of-sight scenarios, avoiding privacy concerns [12]. In particular, the recently exposed channel state information (CSI), which can be obtained from commodity Wi-Fi network interface controllers (NICs), can present subcarrier-level channel measurements. Several CSI-based localization solutions, which may provide sub-meter resolution localization accuracy, were proposed recently [13] [14] [15].

Unfortunately, to the best of our knowledge, a CSI-based DfP localization system for the mobile environment, e.g., ships, is still absent. The existing CSI-based localization approaches fundamentally rely on the assumption that the environment is static, which enables an offline-built localization fingerprints map to be used online for correlating the human locations with the CSI measurements. However, based on our findings (see Sec. 4 for details of experiments), the RF propagation in a mobile indoor environment can be dramatically influenced by the corresponding dynamic outdoor environment factors (such as sailing speed, acceleration motion, turning motion, weather condition, or altitude). In this case, any small change of environmental factors on a ship would dramatically changes the CSI fingerprints and requires updating the entire fingerprint map at all possible sailing conditions, which is (if ever possible) labor-intensive and time-consuming; this makes the system deployment too expensive for any practical setting. The auto-calibration method that self-updates the fingerprint map at runtime, as recently described in [16], cannot guar-

- *M. Chen is with the School of Navigation, Wuhan University of Techology, Wuhan 430063, China (e-mail: chenmz@whut.edu.cn).*
- *K. Liu and J. Ma are with the School of Navigation, Wuhan University of Technology, Wuhan 430063, China, National Engineering Research Center for Water Transport Safety, Wuhan 430063, China and Hubei Key Laboratory of Inland Shipping Technology, Wuhan 430063, China (e-mail: kzliu@whut.edu.cn; majie@whut.edu.cn.*
- *Y. Gu is with Visa, Austin, TX 78759, USA (e-mail: yugu1@visa.com)*
- *Z. Dong is with the Department of Computer Science, Wayne State University, Detroit, MI 48202, USA (e-mail: dong@wayne.edu)*
- *C. Liu is with the Department of Computer Science, The University of Texas at Dallas, Dallas, TX 75080, USA (e-mail: cong@utdallas.edu)*

** Corresponding author: Cong Liu (cong@utdallas.edu).*

antee performance because the ship environment changes unpredictably and instantaneously. Unpredictable dynamic factors (such as sailing speed) would lead to insufficient and delayed calibration of data collected at runtime, which causes unacceptable errors in updating the fingerprint map.

In this paper, we address the problem of indoor localization in the mobile ship environment by answering the following questions: *can we build a DfP localization system that (1) works well in a wide range of mobile environmental conditions, (2) is capable of providing fine-grained location information with high accuracy, and (3) has an affordable system deployment cost (in terms of time consumed for site survey)?* To develop an efficient and practical solution, we first conducted extensive measurements and experiments, including implementing and testing existing localization solutions during several voyages on a real-world cruise ship. By analyzing the experimental data, we identified several key insights that motivated our design. First, among major environmental factors, the ship's speed is the dominating factor that may impact CSI fingerprints. Moreover, the CSI fingerprints for the same ship's speed are found to be stable and consistent. Based on these findings, we design and implement **SWIM**, a **S**peed-aware **W**iFi-based passive **I**ndoor localization system for the **M**obile environment, which is applicable to the mobile environment and improves the meter-level localization accuracy. SWIM is designed to learn the predictive fingerprint variation introduced by environmental speed changes and to reconstruct the original fingerprints in multiple speed scenarios. SWIM can adapt to any runtime speed scenarios and significantly reduce the overall system deployment cost from labor-intensive site survey. Experiments conducted on a real-world ship show that SWIM improves localization accuracy from 63.2% to 82.9% while reducing the overall system deployment cost by 87%, compared with the state-of-the-art localization methods including Pilot [13], PADS [17], PinLoc [8], and AutoFi [16].

In summary, the main contributions of this study are as follows:

- To the best of our knowledge, this is the first work that deals with indoor localization in a mobile ship environment, where the wireless signals are severely affected by deformation of the ship along with different sailing states, which degrade the performance of the state-of-the-art device-free localization techniques.
- By studying the relationship between wireless signal variations and various ship sailing factors (through extensive measurements in a real-world passenger ship), we are the first to identify that the speed of the ship is the dominating factor that may affect the wireless signals. We further demonstrate that the CSI variation maintains a regular distribution when the ship's speed holds.
- We design and implement our device-free meter-level localization system for mobile ship environments, SWIM, on commercial WiFi devices, by recognizing the pattern of the CSI variation for each speed, and we scale the prebuilt fingerprint map into multiple speed scenarios. Experiments show that SWIM can improve the overall localization accuracy by 19% and reduce the system deployment cost by 87%.

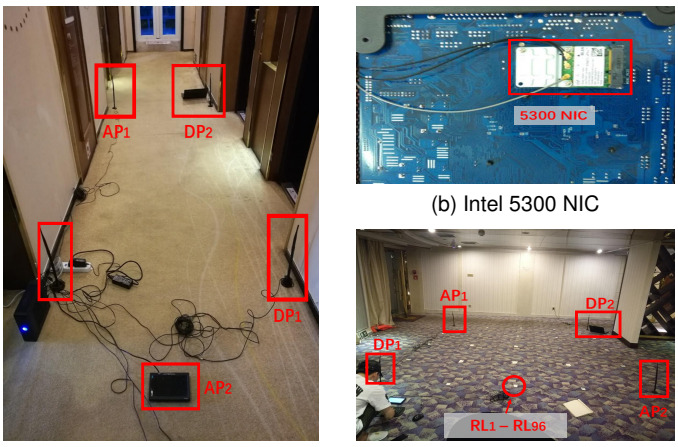

(a) Experiment in corridor (b) Intel 5300 NIC (c) Experiment in hall

Fig. 1. Experiments scenes in passenger ship 'Yangtze 2'.

The rest of the paper is organized as follows. We first describe the motivation of our work in Section 2 and then introduce preliminaries in Section 3. In Section 4, we report the empirical study results about the relationship between the WiFi CSI information and the human activities, followed by the SWIM framework design. Section 6 presents the system performance evaluation results. We review the related work in Section 7. Finally, we conclude our work in Section 8.

2 Motivation

In this section, we motivate our design by showing the unacceptable performance of the state-of-the-art localization solution on a moving ship.

2.1 Setup of the Pilot System

Pilot [13] is a state-of-the-art CSI-based DfP localization scheme, which uses CSI correlations of all subcarriers as a fingerprint to localize targets. It is implemented with commercial IEEE 802.11n NICs and can achieve a meter-level localization accuracy in general indoor scenarios. To evaluate this system, we deployed Pilot on a real-world passenger ship called "Yangtze 2." With the deployment setup described in [13], we conducted experiments in two different indoor ship scenes: a lobby which covers an area of $9.7m \times 13.2m$ and a corridor which covers $1.5m \times 12.8m$. We divided the localization area into square grids. A total of 108 locations were chosen for evaluation. The distance between two neighboring locations was set to be 1 m.

In the experiments, two pairs of detecting points (DPs) and access points (APs) are placed, as shown in Fig. 1. The wireless APs are TP-LINK routers, operating on the 2.4 GHz band with a bandwidth of 20 MHz, to transmit information to DPs. DPs are standard ThinkPad T-series laptops equipped with commercial 802.11n 5300 NICs and the Linux kernel 2.6.34 operating system. To create the localization communication, the DPs constantly pings the APs with a frequency of 10 packets per second (pks). We recruit three volunteers (two male and one female; age: 21—29 years; height: 1.6—1.82 m; weight: 51—90 kg) to perform

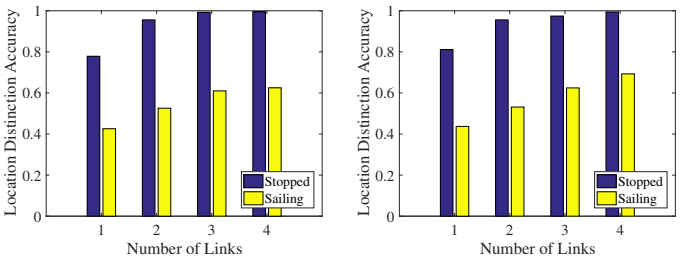

(a) Lobby. (b) Corridor.

Fig. 2. Pilot single entity localization accuracy with different link numbers.

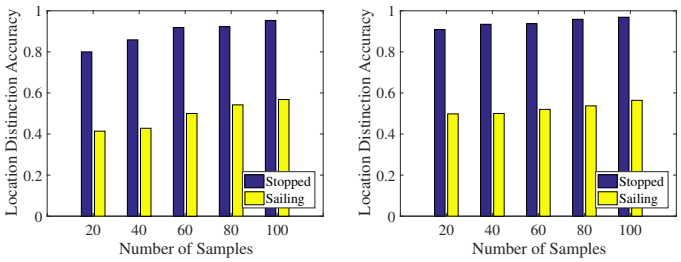

(a) Lobby. (b) Corridor.

Fig. 3. Pilot single entity localization accuracy with different sample numbers.

various daily activities in the two test environments over four ship voyages. According to the procedure of the Pilot system, we recorded the passive CSI fingerprints of each location when the ship was anchored. Then, we tested the system in two environment states:

- **Anchored state**: The Pilot system was evaluated with respect to different numbers of samples collected as fingerprint and different APs when ship anchored. The anchored state test dataset was collected at each location with three volunteers to evaluate the localization performance in Pilot.
- **Sailing state**: To evaluate the system when the ship is moving, we test it again (using the same experimental procedure) after the ship sets sail. The sailing state test dataset was collected during the ship voyage (five days with different sailing conditions).

2.2 Performance of Pilot in indoor ship environment

The results are presented in Fig. 2 and Fig. 3. The performance of Pilot at the anchored ship state is much better than at the sailing state in both lobby and corridor. In the anchored ship environment, Pilot achieves high accuracy, which is similar to the results reported in [13]. As shown in Fig. 2(a), Pilot can achieve over 90% (up to 93.2%) accuracy in the lobby with at least four wireless links. The accuracy increases when aggregating the CSIs from multiple APs. If the number of collected samples increases (from 20 to 100 samples of each location), the accuracy also increases by nearly 10% (up to 9.4%) according to Fig. 3(a). Similar performance is obtained in the corridor scenario. According to Fig. 2(b) and Fig. 3(b), the localization accuracy improves if the numbers of links and samples increase.

However, as the ship starts sailing, the maximum accuracy of Pilot dramatically degrades to 63.2% (in both scenarios) with the maximum number of links and samples. As shown in Fig. 2(a), the location distinction accuracy of Pilot is down to 41.2% with one link. Increasing the APs and collecting samples slightly improves accuracy to 58.9%, which is still largely behind the anchored ship state. The effect of increasing number of samples in the corridor on accuracy is limited, as shown in Fig. 3(b). The experimental results are consistent for two tested locations. This indicates that the sailing state leads to an obvious decrease in localization accuracy of CSI-based passive indoor localization techniques. From empirical experiments in scenarios with two ship states, we can conclude that the Pilot system cannot be directly used in mobile environments such as ships.

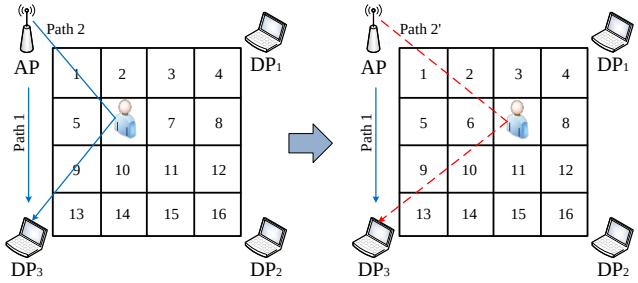

Fig. 4. Illustrate basic idea by collecting CSI fingerprint.

3 Preliminaries

In this section, we explain why existing CSI-based indoor localization techniques lose their accuracy in the mobile ship environment. We start by introducing the necessary background on CSI-based indoor localization techniques.

3.1 Background of CSI-Based Indoor Localization

CSI is a fine-grained physical layer information that describes how the Wi-Fi signals propagate through the wireless channel at the subcarrier level. In the frequency domain, each transmitted symbol $X(f)$ is modulated on a subcarrier frequency f, and the received symbol $Y(f)$ depends on the wireless channel frequency response (CFR) $H(f)$:

$$Y(f) = H(f) \times X(f) \tag{1}$$

CSI is the sample version of the CFR and depicts the amplitude and phase of a subcarrier:

$$H(f_i) = |H(f_i)|e^{jsin(\angle H(f_i))} \tag{2}$$

where f_i is the central frequency of subcarriers ($i = 1, ..., M$), $|H(f_i)|$ denotes its amplitude, and $\angle H(f_i)$ denotes the phase. For each transmission, a group of CSI measurements on M = 30 subcarriers (corresponding to $Ng = 2$ for 20 MHz and $Ng = 4$ for 40 MHz, where Ng is the tone grouping factor) are exported by leveraging a commercial off-the-shelf Intel 5300 NIC with an open source driver [18].

To localize a human by the wireless signal in a passive way, the CSI is used to mark the locations by a location indicator called fingerprints. As shown in Fig. 4, a human

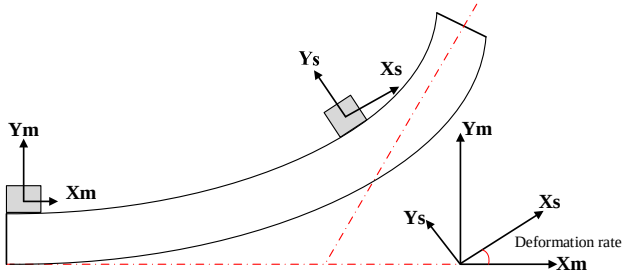

Fig. 5. The deformation caused by dynamic environment.

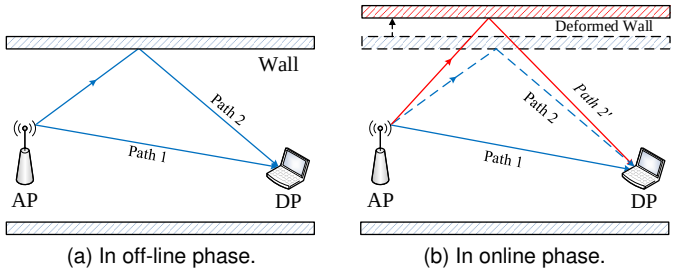

Fig. 6. Illustrate how ship deformation affect wireless signals.

object in the localization space would reflect and absorb the WiFi signals, generating a unique signal propagation paths. Thanks to frequency diversity of CSI, it can reflect the varying multipath reflections and is capable of capturing the unique WiFi features [13]. The fingerprint-based technique is proposed to construct a mapping between the CSIs and location of the human target in advance, which is called a radio map. The radio map construction part is known as the offline phase, and the matching part is known as the online phase. In the offline phase, a human target stays in each location (labeled as 1—16 in Fig. 4) and DPs record the CSIs in a database. In the online phase, the human object can be localized by matching the current CSI information that DP received from the database.

3.2 Problem of Environment Deformation

As discussed above, CSI-based DfP localization techniques explore the slight differences in signal propagation, reflection, and absorption if a human is present in the environment. This technique can be very accurate when a fundamental hypothesis holds: the localization environment is consistent in the offline phase and the online phase.

However, this hypothesis does not hold in a mobile ship environment, which is dynamic and inconsistent. Unlike the static indoor environments (e.g., office building), ships that are built with engines and propellers can also sail in the sea with various speeds. When voyaging, ship's hull is subject to inevitable deformations, including static angular deformation and dynamic (elastic) angular deformation, caused by the external stress of loads, waves, and/or environmental temperature changes [19]. The main reasons for the ship static angular deformations, which can amount to 1°, are the redistribution of freight and fuel on it and non-uniform heating of different parts of the ship under the sun. Dynamic angular deformations, which can be as high as 1°—1.5°, are caused by hull motion, wave impact, helm steering, etc. In recent years, researchers have studied and developed ship's deformation measurement and correction techniques, including the inertial measurement units matching method which is shown in Fig. 5. The practical measurement results show that the values of such deformations for ships are equal to units of angular minutes in the plane of the deck, dozens of angular minutes in the longitudinal central plane, and fractions of an angular minute for the torsion angle. For typical frequency of 0.1 Hz and 0.3 Hz, the angle displacement is obvious [20]. Owing to these deformations (mainly dynamic) of the sailing ship, the angular position of

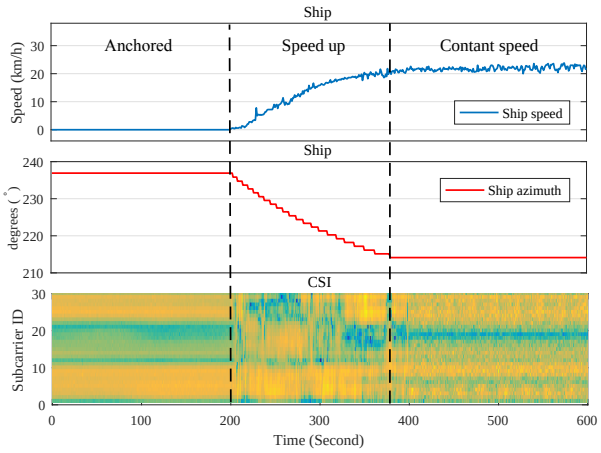

Fig. 7. CSI when stopped vs CSI when sailed.

peripheral equipment (radar antennas, WiFi antennas, optical systems, etc.) may differ significantly from the original devices setup parameters [21].

As a result, with the existing WiFi-based DfP localization solutions such as Pilot, the CSI radio map of all locations is built in the offline phase. During the sailing, the ship's hull deforms and changes the WiFi signal paths, as illustrated in Fig. 6. Thus, the newly detected CSI will become different from those already stored in the database, leading to significant degradation of accuracy.

4 Measurement and Hypothesis

Based on the preliminaries, in this section, we investigate in detail how the ship's sailing affects ship's deformation by observing the measured CSI and ship sensors data. Two hypotheses of the relationship between CSI fingerprint and mobile environment factors are proposed. We validate these hypotheses by extensive measurements in a real-world passenger ship. The hypotheses would provide insight for our eventual system design.

4.1 How Dynamic Environment Affects CSI

We first deployed an AP and DP in the indoor ship environment to monitor WiFi signals. The DP is five meters from the AP and it generates packets every 10 milliseconds on average. We then deployed two smartphones with GPS, accelerometer, gyroscope, and thermometer in the ship to measure and record the ship motion information. To study how CSI behaves under different environmental factors, we

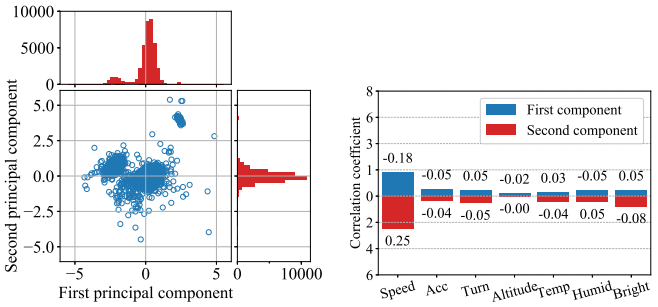

(a) CSI projection to the first two principal components.

(b) Pearson correlation coefficient between CSI projection and ship factors.

Fig. 8. Main influence factor identification in hall.

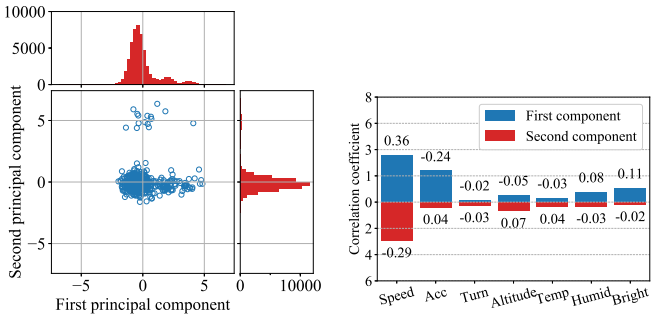

(a) CSI projection to the first two principal components.

(b) Pearson correlation coefficient between CSI projection and ship factors.

Fig. 9. Main influence factor identification in corrdior.

record the CSI and ship sensors data simultaneously. The CSIs and corresponding ships' speeds and headings are plotted in Fig. 7.

According to sensor data, we can divide the process into three phases: the anchored phase, speed up phase, and consistent speed phase. As can be seen in Fig. 7, the CSIs are stable when the ship is anchored. In this phase, the fingerprint-based localization techniques can be very accurate. After the ship starts sailing, we clearly observe that CSI dramatically changes when the ship moves. It implies that the ship's deformation happens when the ship's speed changes. After the ship enters the consistent speed phase, the CSI variation decreased and shows a statistical structure.

4.2 Main Influence Factors of Ship's Deformation

We now present our first hypothesis and the corresponding validation through extensive experimental measurements.

Hypothesis 1: *In all factors that affect ship's deformation, the moving speed of the ship is the dominating influence factor.*

Experiment 1: To verify this, we considered seven environmental factors of a mobile ship scenario. The ship motion factors includes: 1) ship's speed, 2) acceleration, 3) angular velocity, and 4) altitude of ship's location. Outdoor factors are 5) temperature, 6) humid, 7) air pressure, and 8) brightness, which describe the weather. To find the main factor that influences the ship's deformation, indoor WiFi channel state is chosen to measure the slight deformation of the ship indoor environment. Due to the CSI measurements contain multiple subcarriers information, we first adopt an unsupervised technique, namely principal components analysis (PCA) [22], to capture the variation of CSI and reduce the data dimension. Based on the lower dimensional channel states, a supervised univariate feature selection method, called Pearson correlation coefficient, was selected to measure the correlation between each factor with the WiFi channel. The CSI and ship sensor data are simultaneously collected in a passenger room and a meeting room in a real-world ship, as described in Section 4.1.

In each scenario, we collect n packets of CSIs into H, which is $n \times m$ matrix, and m represents the number of subcarriers. The corresponding environmental information is recorded synchronously: ship's speed $V = [v_1, v_2, ..., v_n]^T$, ship's acceleration $A = [a_1, a_2, ..., a_n]^T$, angular velocity of ship's turning $\Omega = [\omega_1, \omega_2, ..., \omega_n]^T$, altitude of ship's location $L = [l_1, l_2, ..., l_n]^T$, temperature of indoor environment $T = [t_1, t_2, ..., t_n]^T$, humid $U = [u_1, u_2, ..., u_n]^T$, air pressure measured by a barometer $B = [b_1, b_2, ..., b_n]^T$, and brightness of the day $D = [d_1, d_2, ..., d_n]^T$.

Before performing PCA, we standardize the CSI matrix H to ensure that all the data are treated on the same scale. The standardized matrix is denoted by $\mathbf{X}$. The PCA attempts to find the projection that best represents the dataset by selecting the maximum-variance directions and transformation matrix A as follows:

$$A_{opt} = \arg\max_{A} |A^T \Sigma A|, \tag{3}$$

where Σ is the covariance matrix of all vectors of $\mathbf{X}$. Solution A is in fact a subset of eigenvectors of Σ as

$$A = [e_1, e_2, ..., e_m], \tag{4}$$

where e_i is the i-th eigenvector obtained from the eigen-decomposition of the matrix Σ. The eigenvalue corresponding to e_i is λ_i, which quantifies the information contributed by the i-th component. The principle components e_i are selected according to the order of eigenvalues λ_i. Based on the transformation matrix A, we can obtain the projection by

$$Y_d = A_{(d)}^T \mathbf{X}, \tag{5}$$

where Y_d is the projection of the d-th component, and $A_{(d)}^T$ is the transpose of the d-th row of the transform matrix A.

After normalizing and filtering the sensors data, Pearson correlation coefficients r can be obtained by:

$$\rho_{Y_i, Z_i} = \frac{\mathbb{E}(Y_i - \bar{Y_i})(Z_i - \bar{Z_i})}{\sigma_{Y_i} \sigma_{Z_i}} \tag{6}$$

where $Y_i \in \{Y_1, \ldots, Y_d\}$ is the CSI projection, and $Z_i \in \{V, A, \Omega, L, T, U, B, D\}$ is the ship sensors' data. $\bar{Y}$ and $\bar{Z}$ represent the mean value of each vector respectively. The value of r is between $[-1, 1]$, which denotes positive or negative correlation.

The results of two scenarios are shown in Fig. 8 and Fig. 9. To visualize the CSI behaviors during the ship sailing, we illustrate the first two components CSI projection (Y_1, Y_2). The eigenvalues of these two components are $\lambda_1 = 7.03$, $\lambda_2 = 6.65$. According to PCA theory, these two components contain most of the information of $\mathbf{X}$, for they

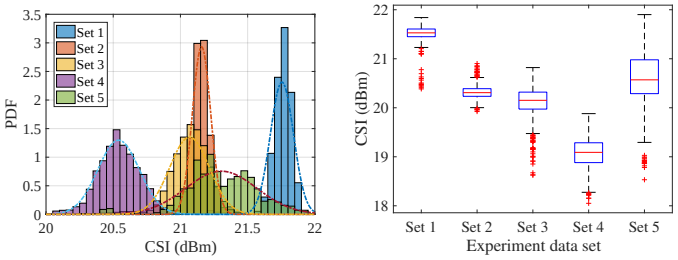

(a) Empirical distribution. (b) Boxplot of CSI distribution.

Fig. 10. CSI measurements of subcarrier #5 under different ship speed of 15 km/h at a same day.

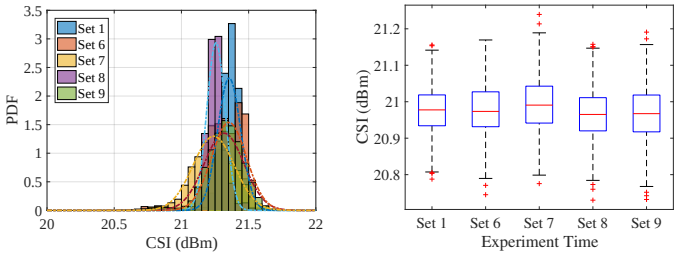

(a) Empirical distribution. (b) Boxplot of CSI distribution.

Fig. 11. CSI measurements of subcarrier #5 under ship speed of 15 km/h at 5 different test time in 3 days.

contribute over 90% of information on the data distribution. The data are scattered in Fig. 8(a) and Fig. 9(a), and the histograms of each component are also shown. The coefficients of each ship factors with these two components projection are calculated and shown in Fig. 8(b) and Fig. 9(b). It can be observed that the speed vector is the most significant factor that influences both Y_1 and Y_2. The coefficient of speed is the highest from seven factors in both scenarios; its influence in the passenger room is higher because of its rich multipath effect in the environment.

These results show that the speed is the dominant factor that affects the ship's deformation and CSI in a mobile ship environment.

4.3 Ship's Speed and CSI Fingerprints

As shown in the experiment from Section 4.1, the CSI tends to be stable after the ship enters the consistent speed state. Based on this observation, we present another hypothesis and its corresponding validation.

Hypothesis 2: *With the same ship's speed, the deformation of the ship is the same, and the CSI can exhibit a regular statistical structure.*

Experiment 2: To verify this, we conducted another set of experiments to inspect if the variant feature of CSIs is stable for a given speed in the same location at different time. Additionally, we record the CSI distributions with different speeds on the same day to examine the speed's effect on CSI fingerprints. Since the tables, chairs, and some windows in the ship are all fixed at the manufacturing phase, the daily environmental changes (moving chairs or opening/closing windows) are not considered in this experiment. The experimental speed and time are described in Table 1. We deploy speed sensors and a pair of AP/DP in the sailing ship to record the ship's speed data and the CSI fingerprints of the same volunteer at a fixed location. Our goal is to inspect whether the CSI fingerprints are the same for a fixed speed. During the experiment, we randomly choose 5 different times during a 3-day window to test the CSI when speed is consistently at 15 km/h both in day and night (Dataset: 1 and 6 to 9). To validate the speed's effect on CSI fingerprint, we record the CSI fingerprints under different speed on the same day (Dataset from 1 to 5). The results are shown in Fig. 10 and Fig. 11.

Gathering all CSIs from all 20,000 packets, the distributions of CSI fingerprints at different speed in one day are first shown in Fig. 10(a): we see huge gaps between each

TABLE 1
Experiments on CSI variation under different speeds and different time.

Set	*Date*	*Time*	*Ship speed*
1	May 3, 2018 (Day 1)	9:00 AM	15.6 km/h
2	May 3, 2018 (Day 1)	1:31 PM	21.2 km/h
3	May 3, 2018 (Day 1)	2:05 PM	6.3 km/h
4	May 3, 2018 (Day 1)	4:34 PM	9.2 km/h
5	May 3, 2018 (Day 1)	10:40 PM	26.1 km/h
6	May 4, 2018 (Day 2)	9:40 AM	15.4 km/h
7	May 4, 2018 (Day 2)	1:21 PM	15.5 km/h
8	May 5, 2018 (Day 3)	10:25 AM	15.2 km/h
9	May 5, 2018 (Day 3)	6:17 PM	15.6 km/h

distribution. The minimum, maximum, mean, and outlier of subcarrier $f = 5$ data are also plotted as a box-whisker plot shown in Fig. 10(b). To be specific, the red line presents the mean of data, while black lines show the minimum and maximum of each CSI with different speed. We see unacceptable variations of fingerprints. On the contrast, we found that the maximum and minimum values are stable in 5 different times of 3 days in the experiments. The CSI distribution of subcarrier $f = 5$ in the speed of 15 km/h is shown in Fig. 11. The Gaussian envelope distributions and boxplot of CSI are also plotted.

The observation is clear: the CSI at the fixed ship's speed exhibits different mean values and variances, but they exhibit stable statistical structures at each subcarrier. That is, the CSI of all subcarriers is relatively stable across different time points when the sailing speed is fixed. This motivates us to design a novel speed-aware CSI-based device-free indoor localization method to achieve high accuracy in the mobile environment. In what follows, we describe our system in detail.

5 The SWIM Design

According to our findings, the elaborated fingerprint map is stable during the same speed. Therefore, to solve the problem of speed's effect, a straightforward solution is to collect the fingerprints for each speed. Apparently, this requires a large system downtime, and the overhead is too high to implement. A better way to solve this issue is to find a speed effect pattern and modify the original CSI fingerprint to adapt to the new speed environments. In this paper, we propose SWIM, a speed-aware 3D fingerprint map generation method to estimate the fingerprints at each speed to cover all deformation effects of the mobile environment. Fig. 12

presents an overview of SWIM. In the following subsections, we will describe each step in detail.

5.1 Base Map Collection

The first step of SWIM is to collect the fingerprint map of the area of interest when the ship is anchored. We call it a **base map**. We define the general fingerprint F_l as a matrix of CSI amplitudes of M subcarriers over all AP links measured by N Wi-Fi packets binding with a location label l. The CSI amplitude vector H_i can be denoted as:

$$H_i = [|H(f_1)^{(i)}|, |H(f_2)^{(i)}|, ..., |H(f_M)^{(i)}|]. \quad (7)$$

The fingerprint F_l is denoted as:

$$F_l = [H_1^{(l)}, H_2^{(l)}, ..., H_N^{(l)}]^T. \quad (8)$$

Unlike previous studies, our study considers the speed factor. SWIM simultaneously collects CSI fingerprints and speed data to obtain the joint CSI-speed fingerprints:

$$F_l^k = \{v_k; F_l\}, \quad (9)$$

where v_k is the instantaneous environmental ship's speed when the fingerprint F_l is measured. We can then denote fingerprints map in all speed scenarios as the joint fingerprints F_l^k. The fingerprint base map (when the speed is 0) is denoted as $\{F_1^0, F_2^0, ..., F_L^0\}$, where L is the total number of locations of the area. In our study, the base map of the mobile ship environment is used to estimate and construct fingerprint maps for each speed in the environment.

5.2 Deformation Function Optimization

As discussed in Sec. 3, the ship's deformation introduced by varying speeds affects CSI and distorts the fingerprints from the base map. To predict the variation of fingerprints at each speed, a set of **reference locations** is selected to measure the changes. Here, P reference locations are adopted: a reference location p is a location that is marked in advance. The fingerprints of location p are collected during the ship sailing at each environment speed and are recorded as:

$$R_p = [F_p^0, F_p^1, F_p^2, ..., F_p^K], \quad (10)$$

where F_p^k is the fingerprint of location l_k at speed v_k.

After obtaining fingerprints of all reference locations at each environmental speed, the effect of ship's deformation on the fingerprint can be denoted as the deformation function $D_p^k(\cdot)$ that describes the relationship of reference fingerprint p between speed k and speed of 0:

$$D_p^k = F_p^k - F_p^0, \quad (11)$$

where F_p^0 indicates the fingerprint of location p when ship's speed is 0. Here, at a certain speed v_k, the effect of ship's deformation on the fingerprint can be presented as the difference between the two CSI-speed joint features. The deformation effect of speed can be rewritten as a mapping function:

$$F_p^k = D_p^k(F_p^0). \quad (12)$$

Here, D_p^k is the deformation function that describes the variation of fingerprints and transforms matrix F_p^0 to a new matrix F_p^k. The deformation function of each speed at calibration location p can be obtained by continuously collecting the speed information and CSI fingerprints:

$$D_p = \{D_p^1(\cdot), D_p^2(\cdot), ..., D_p^K(\cdot)\}. \quad (13)$$

To determine an appropriate form of $D_p^k(\cdot)$, namely **deformation function**, we need to understand the nature of the amplitude variations caused by environmental surface deformation. As illustrated in Fig. 6, environmental surface deformation leads to the effect that some new multipaths appear, while certain old multipaths disappear. According to [16], on each subcarrier frequency, the amplitude of CSI is a combination of signal strength from all multipaths. The new/disappeared multipaths bring a superimposed effect or counteract the effect on all subcarriers. Therefore, for reference location p, we can model the changing function of the i-th subcarrier at speed k as:

$$|H^k(f_i)| = \sum_{j=1}^{M} w_{i,j} |H^0(f_j)|, \quad (14)$$

where the $H^k(f_i)$ is the amplitude of the i-th subcarrier at speed v_k, $H^0(f_j)$ is the amplitude of the j-th subcarrier when speed is 0, M represents the total number of subcarriers, and $w_{i,j}$ is the weight of the j-th subcarrier for estimating the i-th subcarrier. We can obtain F_l^k by multiplying the base map fingerprint F_l^0 by the weight matrix $W = [w_1, w_2, ..., w_M]$:

$$F_p^k = D_p^k(F_p^0, W) = W \cdot F_p^0. \quad (15)$$

After modeling the calibration function, we define the loss function of $D_l^k(\cdot)$ to optimize the best weight of each $W_{i,j}$ in a supervised way by using the reference fingerprints F_p^0 and F_p^k . For the i-th fingerprint point, we define the loss function using the Frobenius norm as:

$$L_i = ||W \cdot F_p^0 - F_p^k||_F^2. \quad (16)$$

The total loss function can be obtained by combining the loss function for each L_i. We extend the loss function with a L2-norm regularization penalty to discourage large weights,

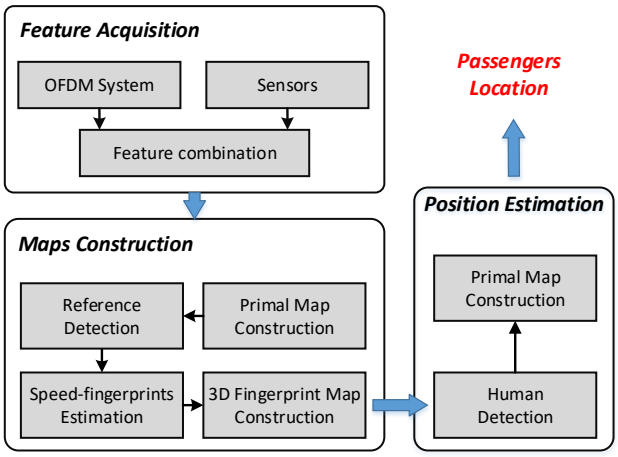

Fig. 12. SWIM overview.

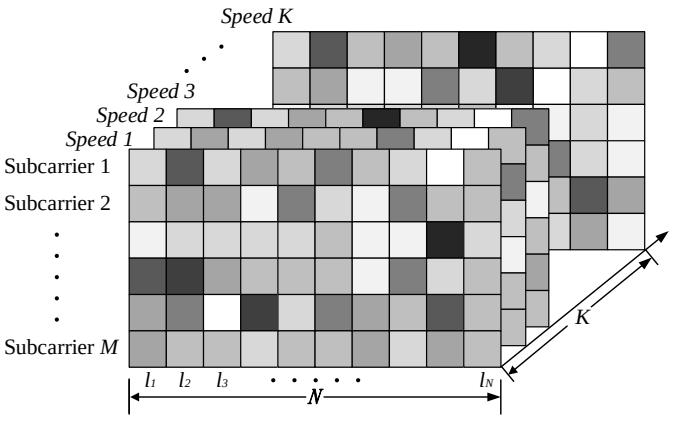

Fig. 13. Speed-CSI 3-D Fingerprint Map.

by using an elementwise quadratic penalty over all weights W:

$$L = \frac{1}{N}\sum_{i=1}^{N} L_i + \lambda \sum_{s}\sum_{t} W_{s,t}^2, \tag{17}$$

where the λ is the regularization factor. We can then calculate the W by the gradient decent method [23]; we skip the details due to limited space:

$$(W_{opt}, b_{opt}) = \arg\min_{(W,b)} L. \tag{18}$$

5.3 3D Fingerprint Map Construction

We now present the core design of SWIM, which can efficiently construct a speed-aware 3D fingerprint map (as illustrated in Fig. 13) using a calibration function to cover all potential speed scenarios without the need of repeating the site survey for each speed.

The **intuition** of the calibration method is that the variation of reference location fingerprint $D_p^k(\cdot)$ indicates a pattern of fingerprint change, which covers an area within valid range d from reference location p as shown in Fig. 14. In other words, using deformation function $D_p^k(\cdot)$, fingerprint change $S_l^k(\cdot)$ of location l, which is within distance d from reference location p, can be approximated as $D_p^k(\cdot)$:

$$D_p^k(\cdot) \cong S_l^k(\cdot). \tag{19}$$

Based on the $S_l^k(\cdot)$, namely **calibration function**, and base map, we can then estimate the fingerprints of all locations at a given speed without physically updating the fingerprint map from scratch:

$$F_l^k = S_l^k(F_l^0), \tag{20}$$

where F_p^0 indicates the fingerprint of location p when ship's speed is 0, and F_p^k represents the fingerprint when ship's speed is v_k. Four real-world fingerprint samples are illustrated in Fig. 15. The fingerprints of reference location at speed of 0 and speed of 10 km/h are shown in Fig. 15(a), and the fingerprints of three nearby test location (2 m, 5 m, and 7m away) are shown in others. The calibration function is trained by using reference fingerprints and tested by the test location fingerprints. As can be seen in the figure, the estimated fingerprints are fit to the ground-truth reference

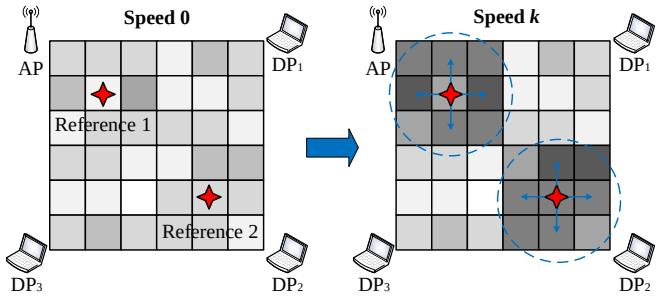

Fig. 14. Speed fingerprint estimation based on reference fingerprint.

fingerprints at speed of 10 km/h. The estimated fingerprint of the test location also fits nicely.

To construct a speed-aware 3D fingerprint map in an efficient way, we consider both the suitable valid distance of the calibration valid range d and the sample scale of the speed dimension v_k ($k = 1, 2, \ldots, K$). To estimate the optimal map parameters, we quantify the distance between two CSI fingerprint sequences. Statistics offers us the Spearman's rank order correlation coefficient [24], which is a metric to rank orders, to capture the similarity of the fingerprint sequences. Given two CSI vectors $F_1 = \{u_i\}$ and $F_2 = \{v_i\}$, $1 \le i \le n$, the metric is defined as the linear correlation coefficient of the elements:

$$\rho = 1 - \frac{6\sum_{i=1}^{n}(u_i - v_i)^2}{n(n^2-1)}. \tag{21}$$

We use the similarity of two neighbor locations fingerprints ε to validate d and v_k. In our measurements, the similarity of estimated speed fingerprint and ground-truth fingerprint is above ε when $d < 5$ m. Similarly, when the speed margin is over 4 km/h, the similarity of fingerprints of the same location would lower to ε and confuse with its neighbor locations. As a result, we choose $d = 5$ m to deploy the reference locations, and set K as 6. The speed dimension v_t is set as $\{v_0 = 0, v_1 = 4$ km/h, $\ldots, v_K = 24$ km/h$\}$. Together with the base fingerprint map and the calibration function, the speed-aware 3D fingerprint map can be constructed accordingly.

5.4 Passive Localization Module

In the previous steps, the offline phase of SWIM collected the base map and estimated the speed-aware 3D fingerprint map based on calibration functions. In the online phase, the CSI and environment speed information are collected continuously and the objects' locations are calculated in real time. We now introduce the passive localization module, which contains two parts.

1) Human Detection: To localize the target in a device-free way, a basic step is to detect the presence of a person in the environment. We design the human detection module to capture environmental changes because of the object's appearance. The system continuously monitors the CSI and calculates the variance that can indicate the appearance of the human object. Denote $H = [|H_1|, |H_2|, ..., |H_N|]$ as the N CSIs sequence. Their corresponding covariance matrix is:

$$\Sigma(H) = [cov(|H_i|, |H_j|)]_{N\times N}, \tag{22}$$

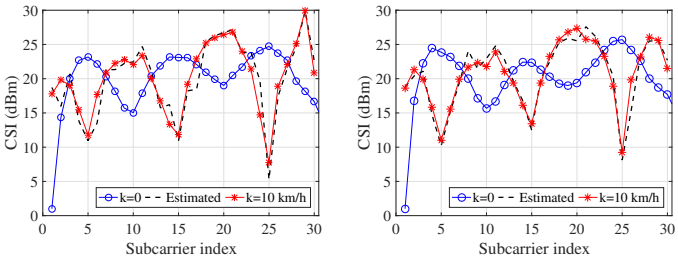

(a) Reference location. (b) Test location of 2 meter distance.

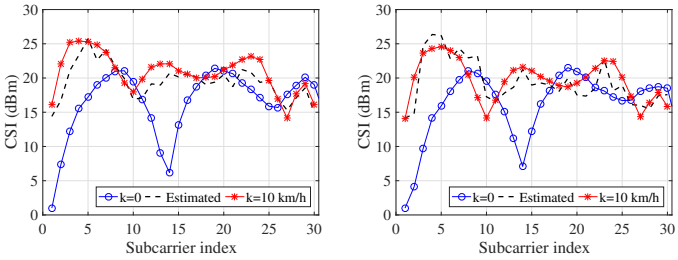

(c) Test location of 5 meter distance. (d) Test location of 7 meter distance.

Fig. 15. Evaluation of fingerprints calibration from speed 0 to 15 km/h.

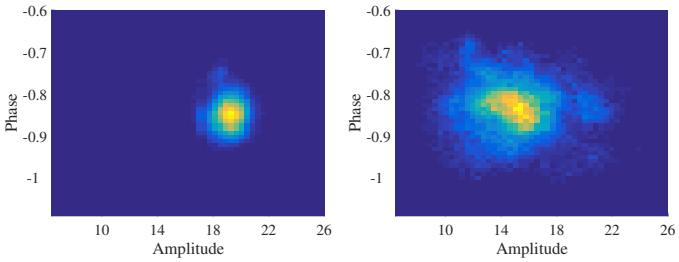

(a) Environment moving. (b) Human moving.

Fig. 16. Variance of CSI of Subcarrier 12.

where $cov(H_i, H_j)$ is the covariance between vectors H_i and H_j.

Fig. 16 shows the variances of subcarrier $f = 12$ when a human is moving or is absent during the ship's sailing. As can be seen, the variance is significantly larger in the former case. Motivated by this observation, we propose a human detection method by comparing the spectral norm (the largest singular value of the matrix) of CSI variances with threshold σ:

$$\begin{cases} P_0: & ||\Sigma(H)||_2 \leq \sigma \\ P_1: & ||\Sigma(H)||_2 > \sigma \end{cases}, \tag{23}$$

where P_0 represents "no human is present" and P_1 is "a human is present." Threshold σ is precalibrated and calculated according to the calibration fingerprints measurements. Once an object event has been detected, it triggers the fingerprint matching process.

2) Position Estimation: We design a device-free fingerprints matching method based on classification with support vector machines (SVM) [25]. SVM is a supervised learning algorithm that uses labeled training data to create a model that can then predict which classes the new test data belong to, given a set of features from the test data. It has also been used in fingerprint-based device-free localization [26].

The SVM used here employs a radial basis function (RBF) kernel to project data to a higher-dimensional space, where the RBF kernel on two samples x and x' is defined as

$$K(x, x') = \exp(-\gamma|x - x'|^2), \tag{24}$$

where γ is a kernel size parameter. We used the open software tool LIBSVM [27] to train and predict the 3D fingerprint map. After identifying the presence of a human in the environment, SWIM reads the current ship's speed data and selects the corresponding SVM classifier to estimate the locations of new fingerprints. The localization procedure is described as Algorithm 1.

Algorithm 1 3D fingerprint map localization.

Input: A CSI sequence, $H = \{H_i\}$; A ship speed v_i;
Output: A boolean variable E denoting whether human exist; The object location L;
Parameters: A variance threshold σ; A buffer length N; A 3D fingerprint map $3DMap = \{v_k : map_k\}$;

```
if len(H) < N then
    return 'Not enough CSI sequence length.';
end if
Σ = Variance(H);
if Σ < σ then
    E = False;
    L = None;
else
    E = True;
    CurrentMap = 3DMap(v_i);
    L = SVMpredict(CurrentMap, H);
end if
return E, L;
```

6 Experiment and Evaluation

We have fully implemented and extensively evaluated SWIM on a real-world passenger ship. We first describe our testbeds and the data collection methodology, and then we evaluate the performance of SWIM against state-of-the-art device-free localization methods.

6.1 Experiment setup

1) Experimental scenarios: We implemented our experimental testbed in "Yangtze 2" passenger ship, which was described in Section 2. Three DPs and one AP are deployed in the area to cover the whole area as shown in Fig. 17. We evaluated 49 locations on this ship for evaluation. The interval between each position is 1 m, which yields a reasonable area for a human to stand. Among these, 2 locations (with a distance of 5 m between them) are selected as reference locations. With these two locations as the centers, circles with a radius of 5 m (which is the reference range in our work) can cover the entire area. At each location, 300 packets of CSI samples are recorded to establish the fingerprints base map. Reference fingerprints are collected within a sailing voyage of the ship, with 300 samples at each speed.

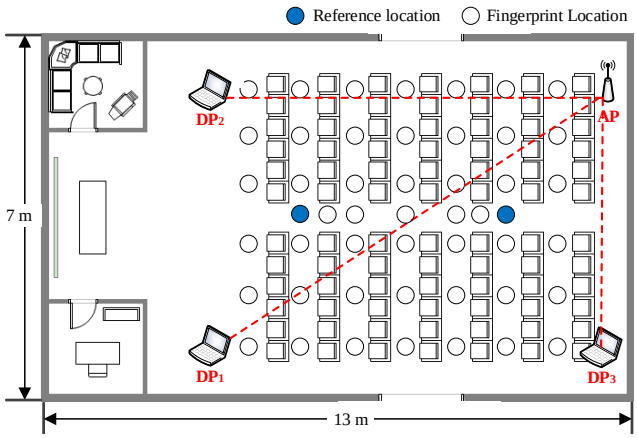

Fig. 17. Fingerprint layout in hall.

2) Comparison techniques: We compare SWIM with three other techniques described in Section 7.

- **Pilot**: Pilot, described in Section 2, uses the CSI correlations of all subcarriers as fingerprints, and the kernel density-based maximum a posteriori probability algorithm to detect and localize a target.
- **PADS**: PADS [17] is a state-of-the-art CSI-based moving target detection method which uses the amplitude and phase information of CSI to extract sensitive metrics for human detection.
- **AutoFi**: AutoFi [16] is a fingerprint-based localization in a changing environment. It can automatically calibrate the localization fingerprint database in an unsupervised manner to adapt to the environment.
- **PinLoc**: PinLoc [8] focused on the fingerprint-based localization using physical layer information in WiFi systems. It can extract the core structure, preserving certain properties useful for localization.

3) Evaluation metric: High accuracy of human detection is necessary to guarantee the efficiency of device-free localization. Thus, we consider two performance metrics: **detection accuracy** and **localization accuracy**.

To quantify the performance of the human detection, we use the following two metrics: true negative rate and true positive rate. Among them, the true negative rate is the probability that the human absence is correctly detected, and the true positive rate is the probability that the human presence is correctly detected. To evaluate the performance of SWIM localization accuracy, we compare the classification accuracies and cumulative positioning error distributions of the methods. A testing CSI fingerprint is accurately localized if its estimated label matches its ground-truth location. We loop through all the testing dataset and collect the average accuracy for each test data sample.

4) Dataset: We recruit 5 volunteers (four male and one female; age: 21—32 years; height: 1.6—1.83 m; weight: 61—82 kg) to perform various daily activities in the ship test environments during five voyages. Each data record consists of a continuous stream of activities, mixing the standing, walking, sitting, and other daily activities with the ship's sensor data. These sensor data include the ship's speed, acceleration, angle, and altitude. We let the subjects to site survey in the experiment scenario. We install a camera to record the ground-truth locations. When the camera records video, the real-time CSI measurements and detection results are updated online. Based on the recorded video and detection results, we can evaluate accuracy of human presence detection and localization. For the reference training set, we have 250 records (from 10 different speed of reference location, 5 daily activities, and 5 people) and 250×300 samples (10 packets per second for 30 seconds).

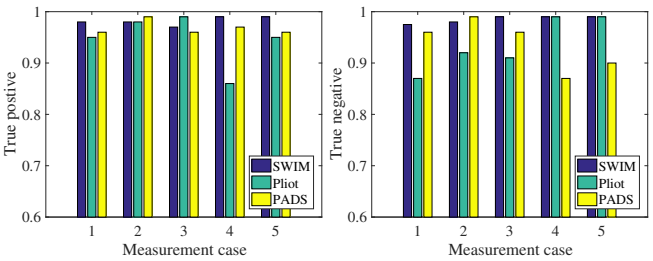

(a) Human exist cases. (b) Human absence cases.

Fig. 18. Comparison of human detection accuracy of three techniques.

6.2 Accuracy of Human Detection

High accuracy of anomaly detection is necessary to guarantee the efficiency of device-free localization. In this section, we evaluate whether SWIM can achieve this goal, and we compare SWIM with the best CSI-based device-free motion detection system PADS and Pilot.

Two methods are compared with SWIM: Pilot and PADS. First, we depict true positive rates of systems when a human is present in the environment. Fig. 18(a) shows the results of five different test cases measured at different times or places. As can be seen, the methods achieve good performances when a human is present in the monitored area. The true positive rates are higher than 98% in most cases. Three systems reach equally high performance in most cases. Among them, PADS and SWIM are more stable than Pilot. Pilot suffers from temporal variance, as indicated by the performance drop in case 4.

Furthermore, we present true negative rates of systems when a human is absent from the environment. As can be seen, PADS and Pilot systems suffer from mobile environment interference, and the true negative rates decreased, which means more false alarms occurred. Fig. 18(b) shows the results of five different cases measured at the same places. PADS and Pilot systems can not only detect human motions precisely but also are sensitive to ship movements. In contrast, our system slightly outperforms two other systems. This validates the effectiveness of our approach for the mobile environment.

6.3 Accuracy of Localization

So far, we have described the performance of human detection in a typical ship scenario. In this part, we discuss localization accuracy as the most important criteria. We show the accuracies of our system and two state-of-the-art techniques: Pilot and AutoFi in ship environment. The accuracy is evaluated with cross-validation of the training and testing dataset, as shown in Fig. 19. The training dataset

is collected in the offline phase. The base map is first collected when the ship is anchored. The passive fingerprints are measured when one volunteer stands on each location. Second, we collect the reference fingerprints and record the ship's speed during ship's sailing. The training dataset is used to 1) estimate the 3D fingerprint map, and 2) train the SVM localization models. The testing dataset is collected in the online phase. One volunteer stands on each location and records the real-time CSI together with ship's speed data. Each testing data point consists of the CSI fingerprint and the current speed. The testing dataset is then passed to the trained model to generate estimated locations. These estimated locations are compared with the ground-truth location for evaluation.

The testing results are shown in Fig. 20. The cumulative localization error of the approaches is plotted. It is shown that the Pilot system performs the worst in the mobile environment, because it is mainly designed for a static environment. The accuracy remains under 90% if the distinction distance is below 4 m. Only after the distinction distance is over 7 m, the Pilot can achieve 99% accuracy, as in a general environment. The AutoFi performs better than Pilot, for it has a calibration module to remove the fingerprints differences from a changing environment. However, for its unsupervised manner, the environment changes cannot be captured completely by its reference fingerprints of an empty area. Here, our system achieves an accuracy of 82.85% when the distinction is 1 m, while Pilot and AutoFi obtain accuracy of 60.52% and 71.31%, respectively. This shows that our system outperforms Pilot and AutoFi in terms of localization accuracy in a mobile environment.

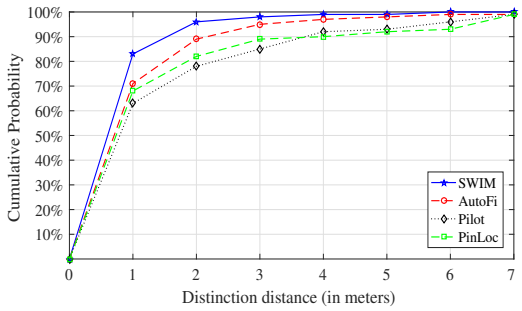

Fig. 20. Localization error distribution.

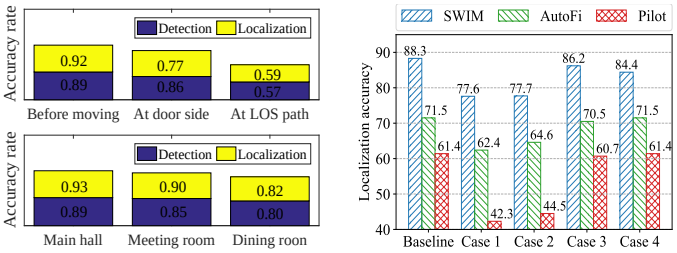

(a) Under impact of moving furniture and different scenarios.

(b) Under impact of other parameters.

Fig. 21. Robustness of SWIM.

6.4 Robustness of SWIM

As the wireless signal is sensitive to the environment, we evaluate the robustness of our approach against setting changes (including opening the door and window, switching on/off the light, moving the furniture around, presence of other humans, and testing in different ship rooms). We will detail the results in the following subsections.

1) Impact of moving the furniture location: To reveal the impact of moving furniture, we move the sofa to different places in the passenger room to evaluate its impact on detection and localization accuracy. The experiment was done under three different conditions: localization is conducted while the sofa is put in the original place (baseline), when the sofa is moved to the door side, and after moving the sofa to the LOS path. We arrange one volunteer to conduct fingerprint collections and reference detection in each of the three scenarios to evaluate the impact of moving furniture on the system performance. The results are shown in Fig. 21(a). Next, we evaluate the robustness of SWIM and get the averaged results as shown in the upper sub-figure. The result shows that when the sofa is moved from the original place to the door side, the human detection accuracy drops slightly from 89% to 86%, and the localization performance drops from 92% to 77%. When the sofa is moved to the room center which blocks the LOS path, the detection accuracy drops significantly from 89% to 57%, and the localization drops from 92% to 59%. It means that the system performance deteriorates under the effect of the big furniture movements, which cause significant CSI change because of variations in wireless signal propagation in multipaths.

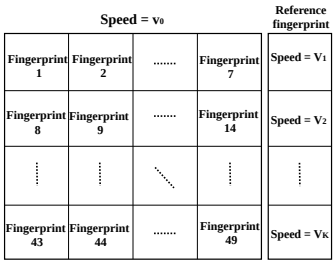

(a) Training data set.

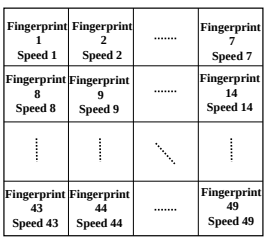

(b) Testing data set.

Fig. 19. Collected data set.

2) System evaluation in different ship scenarios: We then conduct experiments to test the performance of SWIM built for one ship environment in other ship scenarios. The experiment was done under three typical scenarios: the main hall of the passenger ship, the meeting room in the main deck, and the dining room for all passengers. Among them, the main hall has the largest area. The dining room has the most tables and chairs, which results in the most complex multipath effect. In this experiment, we use the same parameters of SWIM tested in the main hall and repeat the procedure described in Section 6.2 and Section 6.3. The result is shown in the lower sub-figure of Fig. 21(a). The detection accuracy changes from 93% in the main hall to 90% and 82% in the meeting room and dining room, respectively; and the localization accuracy drops from 89% in the main hall to 85% and 80% in the meeting room and dining room, respectively. It is obvious that all the system parameters are

TABLE 2
Environment changes and experiments test.

Case	*Environment changes*
$Baseline$	None
1	Human walking
2	Human sitting
3	Opening door
4	Turning on light

environment-dependent, and optimal performance can be achieved by fine-tuning the parameters (calibration valid range and ship's speed margin) in a specific scenario. In summary, the SWIM system is quite robust to small daily changes in the environment. For the significant environmental changes, the system performance can be ensured by fine-tuning the model learned from the changed settings. The result confirms that the meter-level localization system in the ship environment works better in the low-multipath scenario (such as the main hall) than the high-multipath scenario (such as the dining room).

3) Impact of other factors: In this experiment, we check how other parameters of environmental influence may independently affect the system, such as presence of other humans, light turned on/off, and opening of windows/door in the ship. While the WiFi-based system performance may be significantly affected by presence of other humans, we test the robustness of SWIM under such a disturbed environment. The test set of experiments is conducted in four cases: 1) a moving person is walking in the monitored area; 2) two persons are sitting out of the area; 3) randomly opening/closing of the door, and 4) randomly turning on/off the light. Table 2 describes these impact factors in datasets. For all cases, we conducted test experiments in the meeting room during ship sailing and kept the parameters fixed. The results of four cases are shown in Fig. 21(b) with the baseline performance. For the last two cases, the mean localization error achieved by three systems is basically the same as the baseline. SWIM achieves low average localization accuracies of 86.2% and 84.4%, respectively. It can be seen that the WiFi-based systems are not affected by an opened/closed door in the room, as shown in case 3. SWIM is not influenced by the lights as well. The performance is stable when the light is on and off in case 4. However, the system performance varies between cases 1 and 2 because of presence of other humans. We can observe that the performance of SWIM slightly deteriorates to 77.6% and 78.8% when there are humans walking/sitting in the surrounding area. Because SWIM mainly relies on the reflection signal from human bodies, it is sensitive to multipath effects caused by human presence. Presence of other humans would slightly change the WiFi propagation and mislead the fingerprint matching. Therefore, presence of other humans has a larger influence than the other environment parameters (such as light and door) but still less than the influence of the ship's speed.

6.5 Effectiveness of SWIM

We discuss the effectiveness of SWIM from the following two aspects: system deployment cost and energy consumption.

1) System deployment cost: In general, CSI fingerprints are obtained by exploring all the locations manually. We use the time cost of the fingerprints collection to evaluate the deployment cost of SWIM. As described in Section 6.1, the localization area is divided into $1m \times 1m$ grids. Fingerprints of each grid are composed of 200 packets CSI with 0.1 seconds for each measurement. Here, we set a speed margin to be 3 km/h and collect fingerprints at all the speed scenarios. Thus, the fingerprint map establishment time cost for a 10m $\times$ 10m area is at least $(10^2 \times 200 \times 0.1 \times 8)/3600 \approx 4.4$ hours. With SWIM, the only additional cost is the reference fingerprints collection. Thus, the time cost is $((10^2 + (10/5)^2) \times 200 \times 0.1)/3600 \approx 0.57$ hours. In summary, SWIM decreases the overall system deployment cost by approximately 87%.

2) Energy Consumption: SWIM is designed with energy efficiency in mind. Contrary to existing techniques which rely on the active scanning with large power consumption, SWIM uses only beacons from APs in a single channel. For this, it synchronizes with the beacon schedules of these APs and periodically wakes up to collect the CSIs. To this end, it periodically wakes up to collect CSI from APs based on synchronization scheduling. Then, it sends the packet of AP channel states to a central server to perform localization. The amount of such data traffic is low, approximately 1200 bytes per second for 2 APs, and the data upload energy is negligible. To confirm this, we performed measurements on Google Nexus One phones, using the Monsoon power meter. We found that receiving data from 2 APs every 100 ms incurs an additional 5.28 mW power consumption on average. This may be negligible compared to 1326.72 mW on average required to stream a YouTube video.

6.6 Performance under different parameters

In this set of experiments, we evaluate SWIM under varying parameters of calibration valid range and ship's speed sampling.

1) Impacts of calibration valid range: Intuitively, with a longer distance from the reference location, the performance of the calibration function becomes worse. However, with a short valid range, the reference fingerprint detection will require more labor to collect the data. To verify the parameter of calibration valid range used in SWIM, we compare the system performance at different calibration valid range. It can be verified in Fig. 22(a), which presents the change of localization accuracy and detection accuracy against valid range.

The left subgraph of Fig. 22(a) shows that the location recognition rates are higher than 80% when the reference valid range is less than 5 m. It demonstrates that the localization rate is decreased when the range increases, since the variation pattern of the reference location cannot cover the entire localization area, as discussed in Section 5. The right subgraph of Fig. 22(a) depicts the detection rate. As the calibration range decreases, the number of reference fingerprints to calculate the threshold σ is increasing. The result indicates that as long as the calibration valid range is no less than 5 m, which can be easily satisfied in reality, the detection rate is at least 96%.

2) Impacts of ship's speed margin: In practice, the speed of a ship is analog value and needs to be sampled to

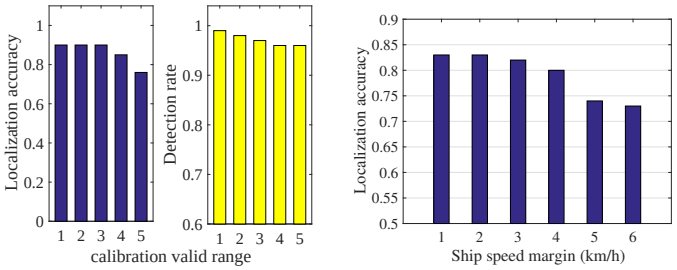

(a) valid calibration range. (b) ship speed margin.

Fig. 22. Relationship of accuracy with valid distance and ship speed margin.

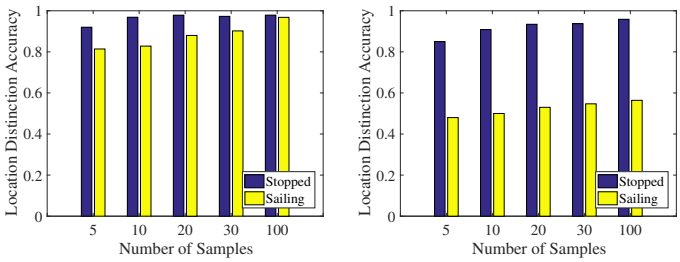

(a) SWIM. (b) Pilot.

Fig. 23. Localization accuracy with different sample numbers.

build the speed-axis of 3D fingerprint map. A dense speed sampling method can achieve sensitive fingerprints and comprehensive knowledge of changing of mobile environment. However, when two speeds of the maps are very close to each other, it is still challenging to accurately distinguish the slight difference between the two maps. If the speed sampling margin is suitably chosen, it can describe location-related information with decreased consumption of memory and computational time. Therefore, the impacts on localization performance of ship's speed margin in SWIM are tested by several speed sampling cases. Here, we increase the margin of ship's speed from 1 km/h to 6 km/h. In Fig. 22(b), the accuracy of 3D fingerprint map of the location under different speed margin is shown. As can be seen in this figure, the system performs well for all the margins which are less than 4 km/h with an average localization error between 80% and 83%.

3) Impact of number of test packets: The test packets, collected in the runtime for localization, affect the fingerprint-based localization system performance according to Section 2. Here we test the localization accuracy of SWIM with different size of the test packets. Assuming that the walking speed of a human is up to 1 m/s and the size of location grids is 1 m, we set the DP extracts CSIs from data packets that are transmitted by APs every 100 ms. Therefore, for localization, we need at least 1 s inside a grid, thereby receiving 10 beacons per AP. Fig. 23 shows the variation of localization accuracy with the number of received packets per AP both in ship sailing and anchored states. With the typical size of 5 packets per AP, SWIM achieves mean accuracy of 82% and Pilot achieves of 47% across 50 locations in the ship main hall when the ship is sailing. 20 packets raise them to 88% and 53%, respectively. This is because one single reading may randomly match with an incorrect location. With 100 test packets, we find the SIWM accuracy is above 96%, and Pilot is less than 60%. This indicates that with the higher user mobility, or with high rate of losing packets, SWIM can sustain a good performance.

7 Related Work

Device-free passive detection or localization have drawn much attention in the past years. In this section, we briefly review the most relevant research on passive motion detection in pervasive wireless environments. Then, the related work of indoor localization in the mobile environment is also introduced.

1) Device-free localization: Device-free approaches release the users from the constraint of carrying devices. They passively detect the signal distortions caused by the physical presence of human bodies, and further infer human locations with this information.

Several RSS-based device-free localization systems have been proposed and achieved low hardware cost for localization. The most well-known RSS-based device-free localization is the RTI [10], which deploys a sensor network around the target area and uses the RSS changes to localize and track a person. Nuzzer [28] used Wi-Fi RSSI as fingerprints to localize a person to one of the fingerprinted locations. RASS [29] detected whether a person enters the area of interest, and presented a support vector regression model to enhance system robustness. However, RSS is inherently a coarse measurement and strong multipath makes the problem even worse [30]. As such, RSS-based device-free localization techniques have difficulties providing high localization accuracy in most environments.

Recently, there is a growing interest in exploring CSI for device-free localization, for it can achieve decimeter-level passive localization using commercial off-the-shelf WiFi devices. Compared with RSS, CSI measurements provide more fine-grained information on each subcarrier with both amplitude and phase information [30]. FILA [31] is the first attempt at leveraging CSI for indoor localization and calculation the locations based on trilateration. PinLoc [8] achieves a 90% localization accuracy by using CSI from multiple subcarriers as location fingerprints. Pilot [13] uses the CSI correlations of all subcarriers as fingerprints and the kernel density-based MAP algorithm to detect and localize a target. LiFS [14] leverages shadowing effect of targets near line-of-sight of links and an accurate power fading model, which is not the same in steel structure environment, to estimate the target's location. From experiments in these works, we can conclude that frequency diversity of CSI helps CSI-based scheme outperform the RSS-based scheme and such advantage is obvious when more RF links are available. However, these techniques rely on the assumption that the environments and the locations of Wi-Fi devices unchanged. In the mobile environment, this assumption could be easily violated because the environment keeps changing under different moving conditions. As a result, the performance of these methods is limited in the mobile environment.

2) Dynamic environment: Because device-free localization systems locate a person in an environment by measuring the changes in received signal on links, the systems' performances are subject to changes in the environment (e.g., people, building layouts).

There are a few previous works that consider dynamic environments. In [32], experiments are performed to quantify how changes in an environment affect accuracy, through a repetitive process of randomly moving an item in a localization environment. RASID [33] improves the detection accuracy by analyzing the RSS features and adopting a non-parametric technique for adapting to environmental changes. LEASE [34] employs a number of additional stationary transmitters and receivers to obtain up-to-date RSS values for updating the maps. LEMT [35] presents a regression analysis based method to learn the temporal relationship between the RSS received by reference locations and that received by the mobile device. LeManCoR [36] presents a location-estimation approach based on Manifold co-Regularization, which can transfer the fingerprint map to adapt to the new environment in the online adaptation phase. These methods are mainly used for the RSS signal and long-term environmental changes, which are not suitable to the mobile environment. The changes in the mobile environment are instantaneously and unpredictable, which is hard to collect enough calibration data in time to update the fingerprint map.

Another related study is AutoFi [16], which proposes an auto-calibration approach to collect the CSI of the empty environment after environment layout changes (open window and moved furniture) and reconstruct the fingerprints in online phase. The performance of AutoFi is not remarkable in the mobile environment compared with general environments because the mobile environment changing are complex and slight compared with the layout changes. In this paper, we mostly focus on constructing a fingerprint map to fit the different speed of the mobile environment. Moreover, our approach, as compared with AutoFi, does not require the empty environment CSI data to calibrate the database in the real-time online phase.

8 Conclusion

In this paper, we design and implement one of the first CSI-based indoor localization system for a mobile ship environment. To the best of our knowledge, this is the first attempt to exploit the characteristics of the mobile environment and study the environmental influence factor of indoor localization. We have conducted extensive experiments to identify the main influence factor of a mobile environment on localization and study the relationship between CSI pattern variation and environmental dynamics. These findings motivate us to design SWIM, which calibrates the fingerprints from only a single speed scenario to multiple speed scenarios through a signal reconstruction analysis. Real-world implementation and evaluation show that SWIM is able to efficiently improve localization accuracy and significantly reduce the system deployment cost for a mobile ship environment.

Acknowledgments

This work was supported by the National Natural Science Foundation of China (NSFC) under Grant No. 51979216, the Major Project for the Technology Innovation of Hubei Province, China, under Grant No.2017AAA120, the Fundamental Research Funds for the Central Universities under Grant No. WUT-2017-YB-031.

References

[1] Z. Meng, D. Yao, L. Bai, Y. Zheng, M. Xue, X. Zhang, K. Zhao, F. Tian, and M. Wang, "Wind estimation around the shipwreck of oriental star based on field damage surveys and radar observations," *Science bulletin*, vol. 61, no. 4, pp. 330–337, 2016.

[2] T. Vairo, M. Quagliati, T. Del Giudice, A. Barbucci, and B. Fabiano, "From land-to water-use-planning: a consequence based case-study related to cruise ship risk," *Safety science*, vol. 97, pp. 120–133, 2017.

[3] K. Liu, M. Chen, E. Cai, J. Ma, and S. Liu, "Indoor localization strategy based on fault-tolerant area division for shipboard surveillance," *Automation in Construction*, vol. 95, pp. 206–218, 2018.

[4] Y. Liu, Z. Yang, X. Wang, and L. Jian, "Location, localization, and localizability," *Journal of Computer Science and Technology*, vol. 25, no. 2, pp. 274–297, 2010.

[5] L. M. Ni, Y. Liu, Y. C. Lau, and A. P. Patil, "LANDMARC: indoor location sensing using active RFID," in *IEEE PerCom*, 2003.

[6] L.-X. Chuo, Z. Luo, D. Sylvester, D. Blaauw, and H.-S. Kim, "RF-Echo: A Non-Line-of-Sight Indoor Localization System Using a Low-Power Active RF Reflector ASIC Tag," in *ACM Mobicom*, 2017.

[7] P. Bahl and V. N. Padmanabhan, "RADAR: An in-building RF-based user location and tracking system," in *IEEE INFOCOM*, 2000.

[8] S. Sen, B. Radunovic, R. R. Choudhury, and T. Minka, "Spot Localization Using PHY Layer Information," *ACM Mobisys*, 2012.

[9] M. Chen, K. Liu, J. Ma, and C. Liu, "Spatio-temporal fingerprint localization for shipboard wireless sensor networks," *IEEE Sensors Journal*, vol. 18, no. 24, pp. 10 125–10 133, 2018.

[10] J. Wilson and N. Patwari, "Radio tomographic imaging with wireless networks," *IEEE Transactions on Mobile Computing*, vol. 9, no. 5, pp. 621–632, 2010.

[11] H. Ma, C. Zeng, and C. X. Ling, "A reliable people counting system via multiple cameras," *ACM Transactions on Intelligent Systems and Technology*, vol. 3, no. 2, p. 31, 2012.

[12] M. Youssef, M. Mah, and A. Agrawala, "Challenges: device-free passive localization for wireless environments," in *ACM MobiCom*, 2007.

[13] J. Xiao, K. Wu, Y. Yi, L. Wang, and L. M. Ni, "Pilot: Passive Device-Free Indoor Localization Using Channel State Information," in *IEEE ICDCS*, 2013.

[14] J. Wang, H. Jiang, J. Xiong, K. Jamieson, X. Chen, D. Fang, and B. Xie, "LiFS: low human-effort, device-free localization with fine-grained subcarrier information," in *ACM MobiCom*, 2016.

[15] Y. Wang, J. Liu, Y. Chen, M. Gruteser, J. Yang, and H. Liu, "E-eyes: device-free location-oriented activity identification using fine-grained wifi signatures," in *ACM MobiCom*, 2014.

[16] X. Chen, C. Ma, M. Allegue, and X. Liu, "Taming the inconsistency of Wi-Fi fingerprints for device-free passive indoor localization," *IEEE INFOCOM*, 2017.

[17] K. Qian, C. Wu, Z. Yang, Y. Liu, and Z. Zhou, "PADS: Passive detection of moving targets with dynamic speed using PHY layer information," in *IEEE ICPADS*. IEEE, 2014.

[18] D. Halperin, W. Hu, A. Sheth, and D. Wetherall, "Tool Release : Gathering 802 . 11n Traces with Channel State Information," *Sigcomm*, vol. 41, no. 1, p. 2011, 2011.

[19] G. W. Jiang, S. H. Fu, Z. C. Chao, and Q. F. Yu, "Pose-relay videometrics based ship deformation measurement system and sea trials," *Chinese Science Bulletin*, vol. 56, no. 1, pp. 113–118, 2011.

[20] F. Sun, C. Guo, W. Gao, and B. Li, "A new inertial measurement method of ship dynamic deformation," *Proceedings of the 2007 IEEE International Conference on Mechatronics and Automation, ICMA 2007*, pp. 3407–3412, 2007.

[21] A. V. Mochalov and O. Jo, "Use of the ring laser units for measurement of the moving object deformations," *Second International Conference on Lasers for Measurements and Information Trans. SPIE*, vol. 4680, no. February 2002, pp. 85–92, 2002.

[22] L. I. Smith, "A tutorial on principal components analysis," Tech. Rep., 2002.

[23] L. Bottou, "Large-scale machine learning with stochastic gradient descent," in *Springer COMPSTAT*. Springer, 2010.

[24] B. P. Flannery, S. A. Teukolsky, W. H. Press, and W. T. Vetterling, *Numerical recipes in C: The art of scientific computing*. Cambridge university press, 1988, vol. 2.

[25] F. Pedregosa, G. Varoquaux, A. Gramfort, V. Michel, B. Thirion, O. Grisel, M. Blondel, P. Prettenhofer, R. Weiss, V. Dubourg *et al.*, "Scikit-learn: Machine learning in python," *Journal of machine learning research*, vol. 12, no. Oct, pp. 2825–2830, 2011.

[26] F. Viani, P. Rocca, M. Benedetti, G. Oliveri, and A. Massa, "Electromagnetic passive localization and tracking of moving targets in a wsn-infrastructured environment," *Inverse Problems*, vol. 26, no. 7, p. 074003, 2010.

[27] C.-C. Chang and C.-J. Lin, "LIBSVM: a library for support vector machines," *ACM transactions on intelligent systems and technology*, vol. 2, no. 3, p. 27, 2011.

[28] M. Seifeldin, A. Saeed, A. E. Kosba, A. El-Keyi, and M. Youssef, "Nuzzer: A large-scale device-free passive localization system for wireless environments," *IEEE Transactions on Mobile Computing*, vol. 12, no. 7, pp. 1321–1334, 2013.

[29] D. Zhang, Y. Liu, X. Guo, and L. M. Ni, "Rass: A real-time, accurate, and scalable system for tracking transceiver-free objects," *IEEE Transactions on Parallel and Distributed Systems*, vol. 24, no. 5, pp. 996–1008, 2013.

[30] Z. Yang, Z. Zhou, and Y. Liu, "From rssi to csi: Indoor localization via channel response," *ACM Computing Surveys (CSUR)*, vol. 46, no. 2, p. 25, 2013.

[31] K. Wu, J. Xiao, Y. Yi, M. Gao, and L. M. Ni, "Fila: Fine-grained indoor localization," in *IEEE INFOCOM*, 2012.

[32] B. Mager, P. Lundrigan, and N. Patwari, "Fingerprint-based device-free localization performance in changing environments," *IEEE Journal on Selected Areas in Communications*, vol. 33, no. 11, pp. 2429–2438, 2015.

[33] A. E. Kosba, A. Saeed, and M. Youssef, "Rasid: A robust wlan device-free passive motion detection system," in *Pervasive computing and communications (PerCom), 2012 IEEE international conference on*. IEEE, 2012, pp. 180–189.

[34] P. Krishnan, A. Krishnakumar, W.-H. Ju, C. Mallows, and S. Gamt, "A system for LEASE: Location estimation assisted by stationary emitters for indoor RF wireless networks," in *IEEE INFOCOM*, 2004.

[35] J. Yin, Q. Yang, and L. Ni, "Adaptive temporal radio maps for indoor location estimation," in *IEEE PerCom*, 2005.

[36] S. Pan, J. Kwok, Q. Yang, and J. Pan, "Adaptive Localization in a Dynamic WiFi Environment through Multi-view Learning." *National conference on artificial Intelligence*, pp. 1108–1113, 2007. [Online]. Available: http://www.aaai.org/Papers/AAAI/2007/AAAI07-176.pdf

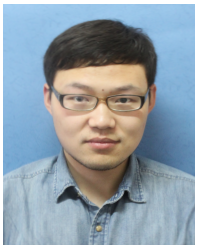

Mozi Chen received the B.S. degree in electric engineering from the Hubei University of Technology, China, in 2013, and the M.S. degree in navigation engineering from the Wuhan University of Technology (WUT), China, in 2016. He is currently a Ph.D. student in WUT. His research interests focused on wireless sensor networks and indoor localization.

Kezhong Liu received the B.S. and M.S. degrees in marine navigation from the Wuhan University of Technology(WUT), Wuhan, China, in 1998 and 2001, respectively. He received the Ph.D. degree in communication and information engineering from the Huazhong University of Science and Techonogy, Wuhan, China, in 2006. He is currently a professor with School of Navigation, WUT. His active research interests include indoor localization technology and data mining for ship navigation.

Jie Ma received the Ph.D. degree in computer science from the Huazhong University of Science and Technology, China, in 2010. He is currently an associate professor in the School of Navigation at the Wuhan University of Technology. His research includes networked sensing systems and data driven intelligent transportation systems, supported by National Natural Science Foundation of China. He has published over 20 journal and conference papers in the related fields.

Yu Gu received the PhD degree from the Department of Computer Science and Engineering, University of Minnesota, in 2010. He is currently the chief architect at Visa. Previously he was a research scientist with IBM Research and Watson Health, Austin. He was an assistant professor with the Singapore University of Technology and Design between 2010-2014. He is the author and coauthor of more than 100 papers in premier journals and conferences. He is a senior member of the IEEE.

Zheng Dong is an assistant professor in the Department of Computer Science at Wayne State University. He received the PhD degree from the Department of Computer Science at the University of Texas at Dallas in 2019. His research interests include real-time cyber physical systems and mobile edge computing. He received the Outstanding Paper Award at the 38th IEEE RTSS. He is a member of the IEEE.

Cong Liu received the Ph.D. degree in computer science from the University of North Carolina at Chapel Hill, in Jul. 2013. He is an associate professor in the Department of Computer Science, University of Texas at Dallas. His research interests include real-time systems and GPGPU. He has published more than 30 papers in premier conferences and journals. He received the Best Paper Award at the 30th IEEE RTSS and the 17th RTCSA. He is a member of the IEEE.